Mean-free path of electrons in rare-gas solids derived from vacuum-uv photoemission data*

Nikolaus Schwentner
Institut für Experimentalphysik der Universität Kiel, Kiel, Germany
(Received 14 July 1976)

The energy distributions of photoelectrons of solid Ar, Kr, and Xe films with thicknesses between 10 and 300 Å have been measured in the photon energy range of 10 to 30 eV using the synchrotron radiation of Deutsches Elektronen Synchrotron (DESY). By varying the photon energy and the film thickness the dependence of the electron-electron scattering length on the electron kinetic energy has been determined. The mean-free path for inelastic electron-electron scattering decreases monotonically from values of the order of 1000 Å at the scattering threshold to values between 1 and 5 Å for electron energies 10 eV above threshold. The observed energy dependence can be understood by a simplified band structure and a scattering probability described by a product of the density of states. The threshold energy for electron-electron scattering lies between twice the energy of the $n = 1$ excitons and the sum of band-gap and exciton energy.

I. INTRODUCTION

There exist several compilations of electron mean free paths[1,2] in a number of metals and semiconductors for a rather large electron kinetic-energy range. For low energies, the results have been attributed to scattering with phonons and imperfections whereas, at higher energies, inelastic interaction between electrons and excitation of plasmons is dominant.[3] For insulators[4] and molecular crystals,[5] hot-electron transport has been studied to a much lesser extent. Up to electron kinetic energies of about 1 eV, information about electron transport properties of solid rare gases is available from mobility measurements[6] and from photoelectron transmission measurements.[7] The dynamic properties of excitonic states have also been studied by photonemission.[7,8] In this paper the electron-electron scattering length $L(E)$ for electrons with energies up to 30 eV above the valence band (i.e., kinetic energies up to 20 eV) is determined from photoelectron energy distribution measurements. The rare-gas solids, which are insulators par excellence, have some outstanding features suggesting extraordinary transport properties for electrons. The large band gaps (9.3 eV for Xe, 21.4 eV for Ne) shift the onset for electron-electron scattering to rather high electron energies because both the primary electron and the scattering partner can only be scattered to allowed empty states. The simple phonon spectrum consisting of only acoustic phonons is expected to contribute little to the dissipation of electron kinetic energy due to the small coupling constant and small energy loss per scattering event. Because of the either small or, in Ar and Ne, even negative electron affinities,[9,10] the efficiency for electron emission is high and even the energy distribution of scattered electrons with low kinetic energy can be studied. Finally, from the strong appearance of excitons in optical spectra[11] and electron-energy-loss measurement,[12] an influence of excitons on the threshold of electron-electron scattering is also anticipated. A knowledge of the electron-electron scattering length $L(E)$ is important for the interpretation of photoemission and low-energy-electron-diffraction data because $L(E)$ determines the probing depth. $L(E)$ can be varied by changing the final-state energy and thus exploited to distinguish between bulk and surface properties. In addition, $L(E)$ gives an upper limit for the coherence length of an excited electron in the solid. Therefore $L(E)$ plays a role in the extended x-ray absorption fine structure as well as in the discussion of photoabsorption by direct or nondirect transitions.

II. EXPERIMENT

The synchrotron radiation of the Deutsches Elektronen-Synchrotron (DESY) at Hamburg in combination with a normal incidence monochromator ($\Delta\lambda \approx 2$ Å) provided vacuum-uv radiation in the photon energy range of 10–30 eV.[13] An ultrahigh-vacuum chamber[14] was equipped with a liquid-helium flow cryostat, a photomultiplier for measurements of the sample reflectivity, an electrostatic electron energy analyzer for electron energy-distribution measurements or, alternatively, a collector providing an electric field of 1000 V/cm for total electron yield measurements. With a constant gas flow at the sample surface, a continuous growth of films of rare-gas solids onto the cold Au substrate (≈10 K) was possible. Polycrystalline samples with film thickness between 10 and 10,000 Å with an accuracy of ≈10 Å were prepared. The thickness was controlled by continuously monitoring the oscillations of the reflectivity in the transparent region of the film during the deposition of

the film. The electron energy analyzer with a resolution better than 0.2 eV was mounted normal to the sample surface accepting electrons within a cone of 2°. The transmission of the analyzer is constant with energy for electron kinetic energies above 2 eV. This was checked by varying the preaccelerating voltage between 5 and 20 V. For thicker films, charging of the films up to several eV was observed, resulting in a shift of the whole EDC to smaller kinetic energies (Fig. 1). This effect was minimized by keeping the total illumination time of the film short. Rare gases of research grade with a purity of 99.9997% for Ar, 99.995% for Kr, and 99.997% for Xe were used and handled under ultrahigh-vacuum conditions.

III. RESULTS

Electron energy-distribution curves (EDC's) of thin films of solid Ne, Ar, Kr, and Xe have been measured for photon energies from near the threshold of photoemission (Xe: 9.7 eV, Kr: 11.9 eV, Ar: 13.9 eV, Ne: 20.4 eV) up to 30 eV. The spectra for photon energies between threshold and approximately twice the energy of the band gap (the region without electron-electron scattering) are published in Ref. 10. Figure 1 shows the EDC of solid Ar, Kr, and Xe for photon energies between an energy somewhat below twice the band-gap energy and 30 eV where electron-electron scattering is important. The counting rate is presented versus the kinetic energy of the electrons. Zero represents the vacuum level of the rare-gas sample. For each substance the counting rates for different photon energies are divided by the incident photon flux, so that they can be directly compared. For Ar and Xe, EDC's have been measured for several thicknesses between 10 and 300 Å. Each spectrum can be divided into two parts. The first part with high kinetic energies (A, B) is due to unscattered electrons which have been directly excited from the valence bands of the rare gas. The structure (A, B) contains information about the band structure as is discussed in Refs. 10, 15. After an inelastic electron-electron scattering event an electron excited from the valence bands will appear in the second part (the hatched region) of the EDC. To determine the threshold of electron-electron scattering one has to take into account the lowest electronic excitations, the excitons (Table II). The kinetic energy of an electron which has been excited from the top of the valence band (right arrow) and has suffered an energy loss corresponding to the excitation of an exciton is marked by E_1 (background see later). The appearance of scattered electrons only below E_1 indicates that there exists a minimum loss energy. The

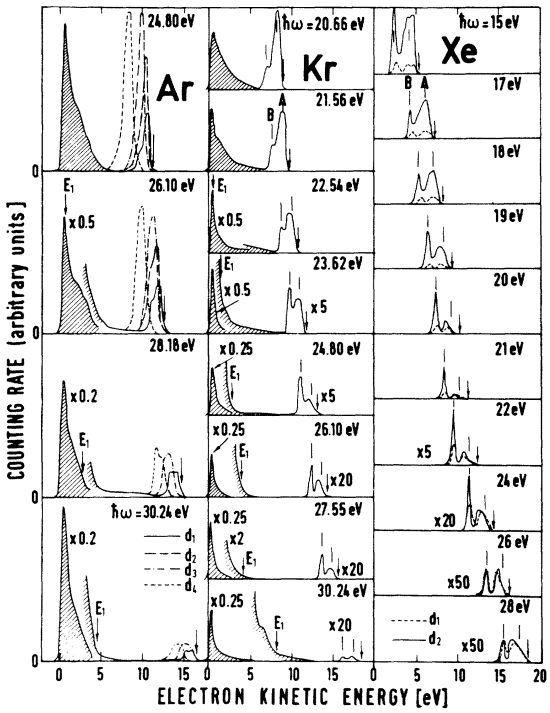

FIG. 1. Photoelectron energy distribution curves of solid Ar, Kr, and Xe films for a spectrum of photon energies $\hbar\omega$. The film thicknesses have been $d_1 = 14$ Å and $d_2 = 228$ Å for Xe (the spectra for $d = 96$ and 426 Å and the region of scattered electrons are not shown) and $d_1 = 30$ Å, $d_2 = 84$ Å, $d_3 = 140$ Å and $d_4 = 300$ Å for Ar. The spectra have been multiplied by the attached factors. For details see text.

threshold for inelastic electron-electron scattering manifests itself in valence-band peaks A, B: For example, in Kr for photon energies between 20.66 and 24.80 eV maximum A is strongly reduced relative to maximum B. Because of the higher kinetic energy of the electrons in maximum A, electron-electron scattering starts at lower photon energies and is stronger thus reducing the intensity relative to B. Parallel to this reduction the ratio of the intensity in the dashed region (with scattered electrons) to the intensity of unscattered electrons grows dramatically for higher photon energies because of the increased production of electrons with low kinetic energy. For photon energies below 20.66 eV, variations in the ratio of maximum A and B are small and can be interpreted in terms of the combined density of states (Refs. 10, 15). Also, the ratio of the dashed region to the region of unscattered electrons shows only weak variation. The analogous behavior is observed for Xe around 18 eV and for Ar around 25 eV indicating that the threshold energy for electron-electron scattering increases with band-gap energy such that the val-

ues are somewhat below twice the band gap. The energy dependence of the electron-electron scattering length $L(E)$ is determined from both the decrease of the counting rate of unscattered electrons associated with a distinct initial energy when the electron kinetic energy is varied through $\hbar\omega$, and also from the thickness dependence of the counting rate of unscattered electrons (Figs. 1, 2). In the left-hand part of Fig. 2, the dependence of maximum A and of maximum B of Kr (Fig. 1) on the kinetic energy of the electrons is shown. Of course, for points at the same kinetic energy, maximum B stems from an EDC of higher photon energy because of the 1 eV deeper initial state. On the right-hand side of Fig. 2, the dependence of the area of unscattered electrons from the EDC's of solid Ar on film thickness is presented for five photon energies. $L(E)$ is calculated using an exponential probability $e^{-x/L(E)}$ for electrons excited at the depth x to reach the surface of the film thus taking into account that only electrons leaving the sample normal to the surface are detected by the analyzer. For an isotropic distribution of electrons the emission $N(E)$ of electrons with kinetic energy E into the angle of acceptance of the analyzer is given by Ref. 16,

$$N(E,\hbar\omega) = Es(E)\, D(E,\hbar\omega)\alpha(\hbar\omega)\int_0^d n(x)e^{-x/L(E)}\,dx\,, \tag{1}$$

where $n(x)$ represents the distribution of photons in a film with thickness d and absorption coefficient $\alpha(\hbar\omega)$ and $Es(E)$ is the escape probability into the analyzer and $D(E,\hbar\omega)$ the local energy distribution at $\hbar\omega$. For the calculation of $n(x)$ one has to take into account interference effects due to reflection of light at the vacuum rare gas and the rare-gas Au substrate interface. The two involved reflectivities R_1 and R_2 are smaller than 10%.[11] To estimate the influence we consider $R_1 = R_2 = 10\%$ and the worst case of a very small absorption coefficient. Interference effects in the film cause a modulation $\Delta R/R$ of sample reflectivity R of $\Delta R/R \approx 0.9$, whereas the modulation of the intensity in the film is only $\Delta n(x)/n(x) \approx 0.1$.

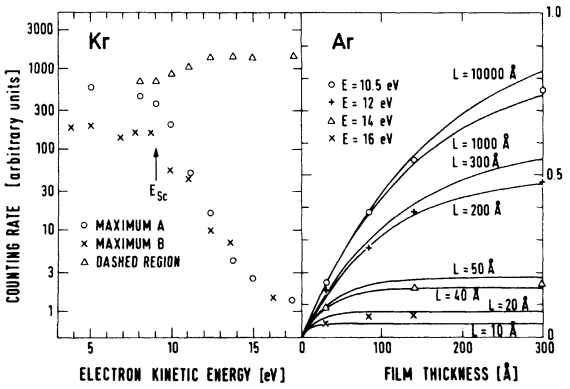

FIG. 2. Left-hand part: Dependence of the intensity of maximum A and B of Fig. 1 on the electron kinetic energy for Kr. 0 corresponds to the vacuum level of Kr. The intensity of the hatched area in Fig. 1 is normalized to the area of unscattered electrons and the energy is attributed to maximum A. Right-hand part: The points show the thickness dependence of the intensity of unscattered electrons from Fig. 1 for Ar. The curves have been calculated according to Eq. (2) using for the different electron kinetic energies the absorption constants given in Table I for the corresponding photon energy. The curves for $L = 1000$ and 10,000 Å and the points for $E = 10.5$ eV have been used to normalize the counting rates (see text).

Therefore $n(x)$ is approximated by $n(x) = e^{-\alpha(\hbar\omega)x}$ Because of the small or even negative electron affinity E_A(Xe: 0.5, Kr: 0.3, Ar: −0.3) and due to the fact that only electrons within a cone of 2° normal to the sample surface are accepted the escape probability is taken as constant for the kinetic energies between 10 and 20 eV. Also the change with energy of the cone of acceptance within the film is neglected. Therefore the escape probability into the analyzer $Es(E)$ can be taken as constant. $D(E,\hbar\omega)$ accounts for the energy distribution of electrons at the site of excitation. $D(E,\hbar\omega)$ is independent of E and $\hbar\omega$ when the counting rate is integrated for the whole area of valence bands, as has been done for Ar on the right-hand part of Fig. 2. Then

$$N(E,\hbar\omega) = EsD\alpha(\hbar\omega)L(E)\{1-\exp[-d[\alpha(\hbar\omega)+1/L(E)]]\}/[1+\alpha(\hbar\omega)L(E)]\,. \tag{2}$$

The crosses and circles for Kr in Fig. 2 show that the counting rate for the parts A and B of the valence bands differ by a factor which is independent of $\hbar\omega$ within the available accuracy. Obviously, at these high energies, changes due to band structure are small and Eq. (2) with constant D values can be used also for different parts of the valence band. Thus one EDC provides results for $L(E)$ at different kinetic energies an advantage also used for the two maxima in the EDC of Xe. By taking $L(E) \geq 1000$ Å [for these high $L(E)$ values the variation of the counting rate as a function of $L(E)$ is

small, see Fig. 2] for $E<16$ eV in Xe, for $E<20$ eV for Kr, and $E<25$ eV for Ar, the proportional constants Es and D for the arbitrary counting rates of Fig. 1 and 2 and Eq. 2 are determined. This procedure seems to be justified by the following reasons:

(a) As has been discussed before the threshold energy for electron-electron scattering lies above these energies.

(b) The counting rate in the dashed region relative to the unscattered electrons contains: (i) hot electrons from the Au substrate excited by transmitted photons and penetrating through the rare-gas film [Fig. 3 and (c)]. The intensity and shape of EDC's from the substrate support this explanation. (ii) Approximately 50% of the electrons excited in the rare-gas film reach the Au substrate and produce secondary electrons with an efficiency increasing with electron energy from 20% to 40%.[17] The secondaries will partly leave the sample yielding an energy distribution similar to an EDC from the Au substrate (cf. Fig. 1). These two contributions explain the intensity, the shape, and the thickness dependence of the counting rate in the dashed region at these low photon energies.

(c) The left-hand part of Fig. 3 shows the transmission of hot electrons through rare-gas films. The electrons are excited in the Au substrate by photons with energies corresponding to the transparent region of the rare-gas film. The total electron yield is measured versus the thickness of the film. The insert gives the EDC of the Au substrate. In this logarithmic presentation of the yield, the slope gives the escape depth L if one simple exponential law is sufficient to describe the electron transport. For thick films ($d \geq 1000$ Å) escape depths of the order of thousand Å are obtained. The finite escape depth is attributed to electron-phonon scattering, electron-impurity scattering, and capture and scattering at defects and crystallite boundaries. The decrease of the escape depth for thin films of Ar may be due to the spectrum of electron energies, the increased probability for backscattering, attraction to the Au substrate by the image potential, changes in the polycrystalline structure of the films, and energy dependence of the phonon emission and absorption probability. The thickness dependence of the absolute yield of Ar from our earlier work[18] is shown in the right-hand part of Fig. 3. The high yield indicates that practically no electrons are lost. The increase of the yield above 0.5 electron per photon absorbed which is unexpected from an isotropic distribution can be explained by either including the secondary electrons from the substrate [see (b)] (solid curves of Fig. 3 for two secondary electron emission coefficients) or by taking into account the increased density of electrons at the surface due to the absorption process. The enhancement of the yield caused by this nonuniform distribution of electrons is shown by a random walk model calculation for three electron-phonon scattering lengths (dashed curves in Fig. 3). For thick films, the random walk contribution will be more important than secondary electrons.

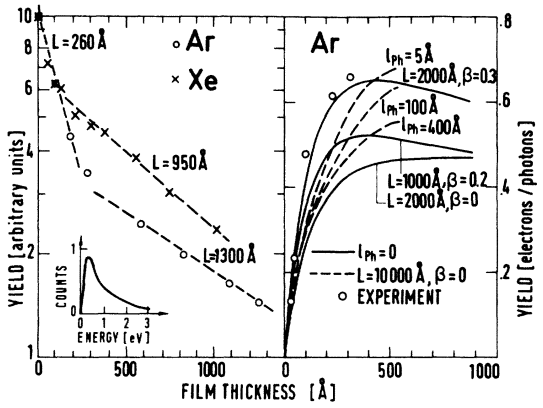

FIG. 3. Left-hand part: Hot-electron current excited in the Au substrate versus Ar and Xe overlayer thickness. The exciting photon energies have been 8.7 eV for Ar and 7.9 eV for Xe. The insert shows the energy distribution of the electrons from the Au substrate for these photon energies. Right-hand part: The circles give the measured absolute electron yield from Ar for different film thicknesses at $\hbar\omega = 18$ eV. The solid curves have been calculated by Eq. (2), including the contribution due to the secondary electron emission coefficient β. From a random walk model calculation using an electron-electron scattering length $L = 10,000$ Å and several electron-phonon scattering lengths l_{ph}, we obtained the dashed curves.

(d) Electron energy loss measurements yield a minimum energy loss equal to the exciton energy.[12] Electron-electron scattering lengths $L(E)$ have been calculated from the results of Fig. 1, with absorption coefficients listed in Table I using Eq. (2). Since the absorption coefficients have not been determined in the whole region, the values of Table I have been taken from Ref. 11 closing the gaps by a smooth connection following the gas values. The results for $L(E)$ of solid Ar, Kr, and Xe are shown in Fig. 4. As is expected from the discussion of the EDC's there is a strong energy dependence in the scattering length. It drops from very high values of several hundred Å near threshold within 2 eV to scattering lengths of the order of 10 Å and within 10 eV to values between 1 and 5 Å. For each kinetic energy L is determined by several independent calculations: (i) from the energy dependence of the counting rate for one maximum of the EDC, (ii) from the thickness dependence for one kinetic energy, (iii) the same kinetic energy ap-

TABLE I. Absorption coefficient used for the calculation of $L(E)$.

$\hbar\omega$ (eV)	$\mu(10^5\ \mathrm{cm}^{-1})$ Ar	Kr	Xe
15			9
17			7.2
18			6.3
19			5.5
20			5
20.66	5	9	
21			4.4
21.56		8	
22			3.7
22.54		7	
23.62		6	
24			2.9
24.80	6	6	
26			2.2
26.10	5	6	
27.55		5	
28			1.65
28.18	4.5		
30			1.25
30.24	4.2	4.5	

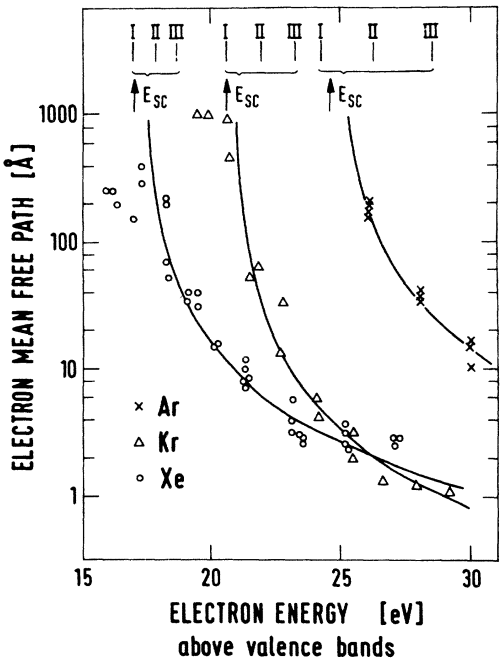

FIG. 4. Electron mean free path versus electron energy measured from top of the valence bands for Ar, Kr, and Xe. The points show the experimental results. The solid curves represent a fit according to Eq. (8). E_{sc} is the electron-electron scattering onset determined by the use of Eq. (8), I corresponds to twice the $n=1$ exciton energy, II to the sum of band gap and $n=1$ exciton energy, and III to twice the band gap for Ar, Kr, and Xe, respectively.

pears in EDC's for different photon energies, and (iv) in each EDC different kinetic energies can be used. Figure 4 demonstrates that the scatter of the points is rather small for Kr and Ar specially for lower L values, whereas it is larger for Xe near threshold. Within the model the main sources of errors are uncertainties in the absorption coefficients and in the film thicknesses. For Kr, the $L(E)$ values are determined from one thickness. An error of a factor of 2 in the thickness would change all the scattering lengths by a factor less than 1.5, and would have only minor influence on the energy dependence of L. For Ar and Kr, errors in the thicknesses will be cancelled as can be seen from Fig. 2. Therefore the most severe errors are introduced by the absorption constants. The scattering of points for Xe does not show a systematic behavior, thus the independent ways of calculating L allow for averaging.

IV. DISCUSSION

First we want to discuss the contribution of electron-phonon interaction to the scattering length. Using an equation given by Baraff[19] the electron-phonon scattering length l_{ph} can be estimated from the escape depth l for electron kinetic energies E greater than the phonon energies E_{ph} in the absence of electron-electron scattering.

$$l_{ph} = 3l(E_{ph}/2E)^{1/2}. \tag{3}$$

Solid rare gases have only acoustic phonons with energies smaller than 10 meV (see Table II). To estimate the order of magnitude of l_{ph} we take mean values of $\bar{E}_{ph}=5$ meV, $\bar{E}=1$ eV (see EDC insert Fig. 3) and $l=1000$ Å and get $l_{ph}=150$ Å. Electron-phonon coupling decreases with the group velocity of the electron therefore for $E>10$ eV the electron-phonon scattering length l_{ph} should be greater than 150 Å. This result is compatible with the increase of the yield with thickness by random walk (Fig. 3) and with the smaller l_{ph} values between 10 and 100 Å measured and calculated for the alkali halides[4] where the coupling of electrons to the optical phonons is expected to be stronger because of the dipole moment of optical phonons.

According to this consideration the influence of electron-phonon scattering is small and $L(E)$ is the electron-electron scattering length: (i) In our EDC's a single electron-phonon scattering event is not considered as an important inelastic scattering event. Because of the small phonon energy the scattered electron would be still in the "unscattered region" of the EDC. (ii) An electron-phonon scattering event only increases the path of the electron to the surface in a random walk process. Due to the small probability of an electron-phonon

TABLE II. Characteristic energies for the electron mean free path (all energies in eV).

		Ar	Kr	Xe
Scattering onset [a]	E_{sc}	24.5	20.5	17
Scattering onset from yield [c]	E_{sc}^{yield}		21.5	17.6
2 times band gap [b]	$2E_G$	28.5	23.2	18.6
band gap plus exciton energy [b]	E_G+E_{ex}	26.25	21.85	17.75
2 times ($n=1$) exciton energy [b]	$2E_{ex}$	24.2	20.5	16.9
constant [a] C [Eq. (8)] (Å eV$^{3/2}$)		100	17	42
maximum phonon energy [e]		0.0083	0.0062	0.0054
plasmon energy [d]		19.2	16.8	14
lowest s excitations [b,c]		~27.4	~25	~20.6

[a] This work from $L(E)$ [Eq. (8)].
[b] Reference 11.
[c] Reference 9.
[d] J. D. Nuttall, T. E. Gallon, M. G. Devey and J. A. D. Matthew, J. Phys. C 8, 445 (1975).
[e] For a recent review, see M. L. Klein and T. R. Koehler, in *Lattice Dynamics of Rare Gas Solids in Rare Gas Solids* I, edited by M. L. Klein and J. A. Venables (Academic, New York, 1976).

scattering event within the electron-electron scattering mean free path above E_{sc} also this contribution may be negligible. The weak electron-phonon interaction explains the steep EDC of "unscattered" electrons. Structures in the EDC's caused by excitations of the deeper lying s levels or of plasmons (Table II) have not been observed.

Second a model is presented for the energy dependence of $L(E)$. As was first proposed and used by Berglund and Spicer[20] for Cu and later confirmed by calculations of Kane[21] the complex scattering problem with full conservation of momentum exchange can be reduced to an integration of the density of states. This simplification works because of the averaging effect of the great variety of possible scattering events contributing to $L(E)$. The probability $P_s(E,E')$ for scattering of the primary electron at E to the lower energy E' by exciting an electron from the valence band E'' to $E'''=E''+E-E'$ is given by

$$P_s(E,E')=\frac{2\pi}{\hbar^2}\int_{VB}|M|^2\rho_{CB}(E')\rho_{VB}(E'')\rho_{CB}(E''')dE'', \tag{4}$$

where $\rho_{VB}(E)$, $\rho_{CB}(E)$ are the density of states of the valence and conduction bands, and M the matrix element which has been assumed to be constant. The inverse lifetime or total scattering probability $P(E)$ follows as

$$P(E)=\int_{E_G}^{E-E_G}P_s(E,E')dE'. \tag{5}$$

Further, a very simple band structure for the rare-gas solids has been used by neglecting the width of the valence bands and by taking parabolic conduction bands $\rho_{CB}\propto(E-E_g)^{1/2}$ separated from the valence bands by the gap energy E_G, which may be reasonable due to the averaging effect of Eq. (5). Thus

$$P(E)=C''\int_{E_G}^{E-E_G}\rho(E')\rho(E-E')dE'=C'(E-2E_G)^2. \tag{6}$$

From $L(E)=v_g(E)/P(E)$ [$v_g(E)$ is the electron group velocity] $L(E)$ follows as

$$L(E)=C'(E-E_G)^{1/2}(E-2E_G)^{-2}. \tag{7}$$

The experiments yield a threshold energy for electron-electron scattering smaller than $2E_G$ because also excitons can be created. Therefore the full lines in Fig. 4 have been calculated for the best fit of C and E_{sc} from the equation

$$L(E)=C(E-E_G)^{1/2}(E-E_{sc})^{-2}. \tag{8}$$

The calculated curves follow the experimental values, for C and E_{sc} see Table II. To test the calculated energy dependence Fig. 5 gives a double logarithmic plot of L vs $E-E_{sc}$. The variation of $(E-E_G)^{1/2}$ is small at such high energies therefore the calculated curves are almost straight lines with a slope of -2. As can be seen this energy dependence fits the experimental results quite well. Of course, at higher energies the matrix elements and additional scattering channels will change the energy dependence of L. The dashed line represents an example for Kr of the prediction of a semiempirical model which was developed for the ionization cross section of gases at high energies[22] and which was adopted also to solids.[23] At threshold neither the energy dependence nor the absolute values agree with the experiment. Finally, the threshold energy E_{sc} will be discussed.

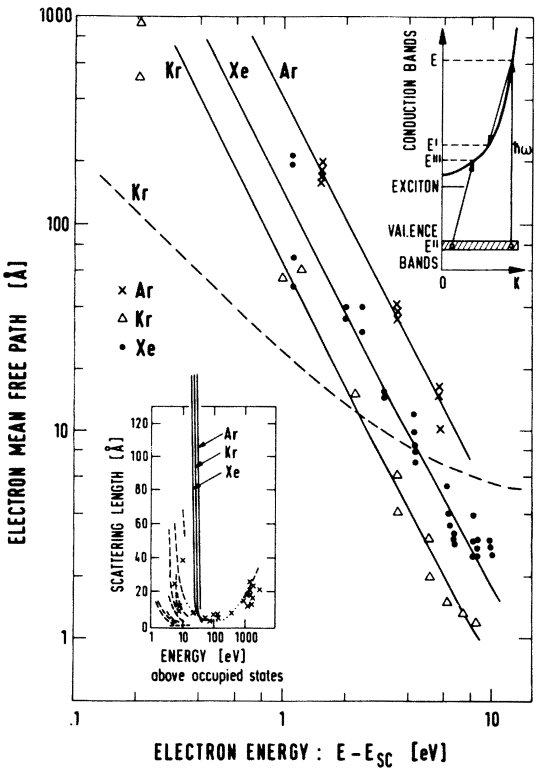

FIG. 5. Electron mean free path versus energy above scattering onset E_{sc} in a double log plot. The points give the experimental results of Fig. 4 and the solid curves the fit due to Eq. (8). The lower insert compares the electron mean free path of Ar, Kr, and Xe determined in this work with the scattering length of other materials (see Ref. 1). The upper insert shows a scheme of the energies involved in the calculation of the mean free path [Eq. (8)]. For further details see text.

Table II demonstrates that E_{sc} is definitely smaller than twice the band-gap energy and that it lies near $E_G + E_x$, the sum of band gap and energy of the first exciton. At E_{sc} the primary electron can be scattered down to the bottom of the conduction band by exciting an exciton. See also E_1 in Fig. 1. Also in total yield measurements[9] at $E_G + E_x$ a decrease in efficiency has been observed. It seems interesting that in Xe, Kr, and Ar, E_{sc} is even smaller than $E_G + E_x$. This may be partly due to the fact that E_{sc} is taken from Eq. (8) and that the excitons have a low-energy tail.[11] But at least in Kr the threshold energy corresponds to twice the exciton energy. In alkali halides, structures due to an excited bound electronic polaron complex with a threshold energy of approximately twice the exciton energy have been suggested for the explanation of several structures in absorption spectra.[24] This theory would postulate the excitation of two excitons in the primary process. As a consequence the number of electrons with high kinetic energy ("unscattered electrons") would decrease and according to our evaluation this would simulate an onset of scattering at this energy. The evidence from $L(E)$ seems to be too weak to definitely identify this process. Perhaps luminescence measurements, which are sensitive to the creation of additional holes may clarify this point.[25]

The insert in Fig. 5 shows a comparison of $L(E)$ for rare-gas solids with some other materials. The references have been taken from Ref. 1. The striking point is the large energy range free from electron-electron scattering and the very steep decrease of L near threshold. Some eV above the threshold L reaches values near the so-called "universal curve."

ACKNOWLEDGMENT

It is a pleasure to thank Professor W. Steinmann and Dr. M. Skibowski for initiating this work and Dr. E. E. Koch, V. Saile, F.-J. Himpsel, and D. Pudewill for strong experimental support and stimulating discussions.

*Work supported by the Deutsches Elektronen-Synchrotron DESY and the Deutsche Forschungsgemeinschaft DFG.

[1]I. Lindau and W. E. Spicer, J. Electron. Spectrosc. 3, 409 (1974).

[2]C. J. Powell, Surf. Sci. 44, 29 (1974); M. Klasson, A. Berndtson, J. Hedman, R. Nilson, R. Nyholm, and C. Nordling, J. Electron. Spectrosc. 3, 427 (1974).

[3]J. J. Quinn, Phys. Rev. 126, 1453 (1962); H. Kanter, Phys. Rev. B 1, 522 (1970).

[4]V. N. Shchemelev, M. A. Rumsh, and E. P. Denisov, Sov. Phys.-Solid State 5, 827 (1963); S. W. Duckett and P. H. Metzger, Phys. Rev. 137, A953 (1965); W. Pong, J. Appl. Phys. 37, 3033 (1966); J. Llacer and E. L. Garwin, J. Appl. Phys. 40, 2766 and 2776 (1969); D. Blechschmidt, M. Skibowski, and W. Steinmann, Phys. Status Solidi. 42, 61 (1970); T. Lewowski, P. Bastie, and M. Bizouard, Phys. Status Solidi. A 2, 847 (1970); I. R. McDonald, A. M. Lamki, and C. F. G. Delaney, J. Phys. D 6, 87 (1973); A. D. Baer and G. J. Lapeyre, Phys. Rev. Lett. 31, 304 (1973); E. L. Battye, J. Liesegang, R. C. G. Leckey, and J. G. Jenkin, Phys. Rev. B 13, 2646 (1976).

[5]P. G. Fuochi and G. R. Freeman, J. Chem. Phys. 56, 2333 (1972); Y. C. Chang and W. B. Berry, *ibid.* 61, 2727 (1974); Jan-Tsyu J. Huang, and John L. Magee, *ibid.* 61, 2736 (1974).

[6]W. E. Spear, Adv. Phys. 23, 523 (1974).

[7]Z. Ophir, B. Raz, J. Jortner, V. Saile, N. Schwentner, E. E. Koch, M. Skibowski, and W. Steinmann, J. Chem. Phys. 2, 650 (1975); Z. Ophir, N. Schwentner, B. Raz, M. Skibowski, and J. Jortner, *ibid.* 63, 1072 (1975).

[8]N. Schwentner and E. E. Koch, Phys. Rev. B (to be published); D. Pudewill, F.-J. Himpsel, V. Saile, N. Schwentner, M. Skibowski, E. E. Koch, and J. Jortner, J. Chem. Phys. (to be published).

[9]N. Schwentner, M. Skibowski, and W. Steinmann, Phys. Rev. B 8, 2965 (1973).

[10]N. Schwentner, F.-J. Himpsel, V. Saile, M. Skibowski, W. Steinmann, and E. E. Koch, Phys. Rev. Lett. 34, 528 (1975).

[11]For a recent review, see B. Sonntag, in *Dielectric and Optical Properties in Rare Gas Solids*, edited by M. L. Klein and J. A. Venables (Academic, New York, to be published).

[12]P. Keil, Z. Phys. 214, 251 and 266 (1968); J. D. Nuttall, T. F. Gallon, M. G. Devey, and J. A. D. Matthew, J. Phys. C 8, 445 (1975).

[13]E. E. Koch and M. Skibowski, Chem. Phys. Lett. 9, 429 (1971).

[14]N. Schwentner, A. Harmsen, E. E. Koch, V. Saile, and M. Skibowski, in *Vacuum Ultraviolet Radiation Physics*, edited by E. E. Koch, R. Haensel, and C. Kunz (Pergamon, Vieweg, 1974).

[15]A. B. Kunz, D. J. Mickish, S. K. V. Mirmira, T. Shima, F.-J. Himpsel, V. Saile, N. Schwentner, and E. E. Koch, Solid State Commun. 17, 761 (1975).

[16]S. V. Pepper, J. Opt. Soc. Am. 60, 805 (1970).

[17]R. L. Petry, Phys. Rev. 28, 362 (1926).

[18]E. E. Koch, B. Raz, V. Saile, N. Schwentner, M. Skibowski, and W. Steinmann, Jpn. J. Appl. Phys. Suppl. 2, 775 (1974).

[19]G. A. Baraff, Phys. Rev. 135, A528 (1964).

[20]C. N. Berglund and W. E. Spicer, Phys. Rev. 136, A1030 (1964).

[21]E. O. Kane, Phys. Rev. 159, 624 (1967).

[22]W. Lotz, Z. Phys. 206, 205 (1967).

[23]F. L. Battye, J. G. Jenkin, J. Liesegang, and R. C. G. Leckey, Phys. Rev. B 9, 2887 (1974).

[24]J. T. Devreese, A. B. Kunz, and T. C. Collins, Solid State Commun. 11, 673 (1972).

[25]H. Möller, R. Brodmann, U. Hahn, and G. Zimmerer (unpublished).